CHEMISTRY
A EUROPEAN JOURNAL

DOI: 10.1002/chem.200800910

Screening Electronic Communication through *ortho*-, *meta*- and *para*-Substituted Linkers Separating Subphthalocyanines and C_{60}

David González-Rodríguez,[b] Tomás Torres,*[b] María Ángeles Herranz,[c, d] Luis Echegoyen,*[c] Esther Carbonell,[a] and Dirk M. Guldi*[a]

Abstract: We have prepared two complementary series of SubPc–C_{60} (SubPc = subphthalocyanine) electron/energy donor–acceptor systems, in which the two constituents are linked through *ortho*-, *meta*-, or *para*-substituted phenoxy spacers. In one of the series (**1a**) the SubPc units bear iodine atoms, while in the other series (**1b**) diphenylamino groups are linked to the SubPc macrocycles. The iodine atoms and diphenylamino groups both influence the resulting oxidation potentials of the electron-donating SubPc. They also modulate the outcome of excited state interactions, namely, energy and/or charge transfer. In addition, we have studied the impact that the substitution pattern in the phenoxy spacer exerts onto intramolecular processes in the ground and excited states. Although some of these processes are governed by the spatial separation between both components, the different electronic coupling through *ortho*-, *meta*-, or *para*- connections also plays decisive roles in some cases.

Keywords: donor–acceptor systems · electron transfer · energy transfer · fullerenes · subphthalocyanines

Introduction

Testing molecular model systems—composed of electron-donating and electron-accepting constituents—assists in understanding factors that ultimately influence photoinduced energy- and electron-transfer reactions.[1] The importance of energy and/or electron transfer is undisputed, since these two primary events govern the conversion of solar energy into profitable chemical energy in natural photoactive reaction centers.[2] They also play a critical role in the performance of, for example, organic solar cells.[3] Usually, well-defined spacers are chosen to connect donors and acceptors. Their nature, which may include covalent or noncovalent, π-conjugated or nonconjugated, rigid or flexible, and so forth, determines the degree of electronic communication, the distance, and the relative orientation.[4] In this context, π-conjugated systems stand out as spacers to afford excellent electronic couplings and, consequently, to accelerate intramolecular events between the two active components.[5] Besides, they may allow switching or fine-tuning of the electronic communication.[6,7]

Recent studies have illustrated the kinetic dependencies of intramolecular processes on the *ortho*, *meta*, or *para* connections in rigid, isomeric, phenyl spacers. These spacers regulate the distance between the donor and acceptor and, consequently, intramolecular processes that occur by means of through-space mechanisms will be favored in the following order: *ortho* > *meta* > *para*.[8] Appreciable differences emerge for the electronic couplings in the isomeric forms. In particular, in systems in which intramolecular events are driven by through-bond interactions (i.e., the π and σ bonds

[a] Dr. E. Carbonell, Prof. Dr. D. M. Guldi
Department of Chemistry and Pharmacy &
Interdisciplinary Center for Molecular Materials (ICMM)
Friedrich-Alexander-Universität Erlangen-Nürnberg
91058 Erlangen (Germany)
Fax: (+49) 9131 8528307
E-mail: dirk.guldi@chemie.uni-erlangen.de

[b] Dr. D. González-Rodríguez, Prof. Dr. T. Torres
Departamento de Química Orgánica
Facultad de Ciencias, Universidad Autónoma de Madrid
Cantoblanco, 28049 Madrid (Spain)
Fax: (+34) 91-497-3966
E-mail: tomas.torres@uam.es

[c] Dr. M. Á. Herranz, Prof. Dr. L. Echegoyen
Department of Chemistry, Clemson University
South Carolina 29634 (USA)
E-mail: luis@clemson.edu

[d] Dr. M. Á. Herranz
Current address:
Departamento de Química Orgánica
Facultad de Ciencias Químicas
Universidad Complutense de Madrid, 28040 Madrid (Spain)

Supporting information for this article is available on the WWW under http://dx.doi.org/10.1002/chem.200800910.

WILEY InterScience DISCOVER SOMETHING GREAT
© 2008 Wiley-VCH Verlag GmbH & Co. KGaA, Weinheim

of the spacer) direct linkages across *meta* positions are less effective than linkages across *para* positions. A reasonable interpretation for this finding is lent from the superexchange mechanism,[9] which leads to a stronger increase in coupling at the *ortho* and *para* positions relative to that at the *meta* connections. Leading examples include singlet–singlet and triplet–triplet energy transfer,[10] photoinduced charge separation and charge recombination,[11] charge transfer to electrodes,[12] or electronic communication in conjugated dendrimers[13] and intervalence metal complexes.[14]

In addition, some of these studies reveal that *meta* linkers may provide enhanced electronic coupling in the excited state, operating as a gated wire in π-conjugated systems.[13] This effect has been demonstrated in conjugated donor–acceptor systems, in which the *meta* connection yielded faster charge separation and slower charge recombination rates than the *para* connection.[11e]

Subphthalocyanines[15] (SubPc's) are nonplanar aromatic macrocycles that exhibit interesting optical properties.[16] Our recent work focused on the synthesis and physicochemical features of subphthalocyanine/fullerene, electron donor–acceptor systems[17] (SubPc–C_{60}). In this work the two photo- and redox-active units were connected by *meta* phenoxy spacers.[17b] Selective photoexcitation of SubPc gave rise—depending on the type of SubPc—to either an energy- or charge-transfer mechanism to yield either a photoexcited or one-electron reduced fullerene, respectively, as a reactive intermediate. The outcome between these two competitive processes was found to depend on the peripheral substitution on the SubPc macrocycle. Donor groups, including phenyl ether or diphenylamino groups, led to a considerable lowering of the SubPc oxidation potentials and, in turn, assisted in favoring electron transfer. However, only energy transfer was operative when the SubPc macrocycle was endowed with fluorine or iodine substituents.

Herein we describe the synthesis of two complementary series of SubPc–C_{60} energy/electron donor–acceptor systems, in which the two constituents are linked through *ortho*-, *meta*-, or *para*-substituted phenoxy spacers. In one of the series (**1a**) the SubPc units bear iodine atoms,[17a] while in the other series (**1b**) diphenylamino groups are linked to the SubPc macrocycle. A wide range of electrochemical and photochemical experiments were employed to probe ground and excited state interactions, as a function of substitution pattern in the spacer, that range from energy- to electron-transfer reactions. We demonstrate that, while some of these processes are clearly regulated by the separation distance between both components, the different electronic coupling through *ortho*-, *meta*-, or *para*- connections can also play an important role in some cases.

Results and Discussion

Synthesis: The synthesis of **1a** and **1b** was carried out by employing triiodoSubPc **4a**[16b] as a common synthetic precursor (Scheme 1). The axial chlorine atom was first replaced by *ortho*-, *meta*-, or *para*-formylphenoxy ligands,

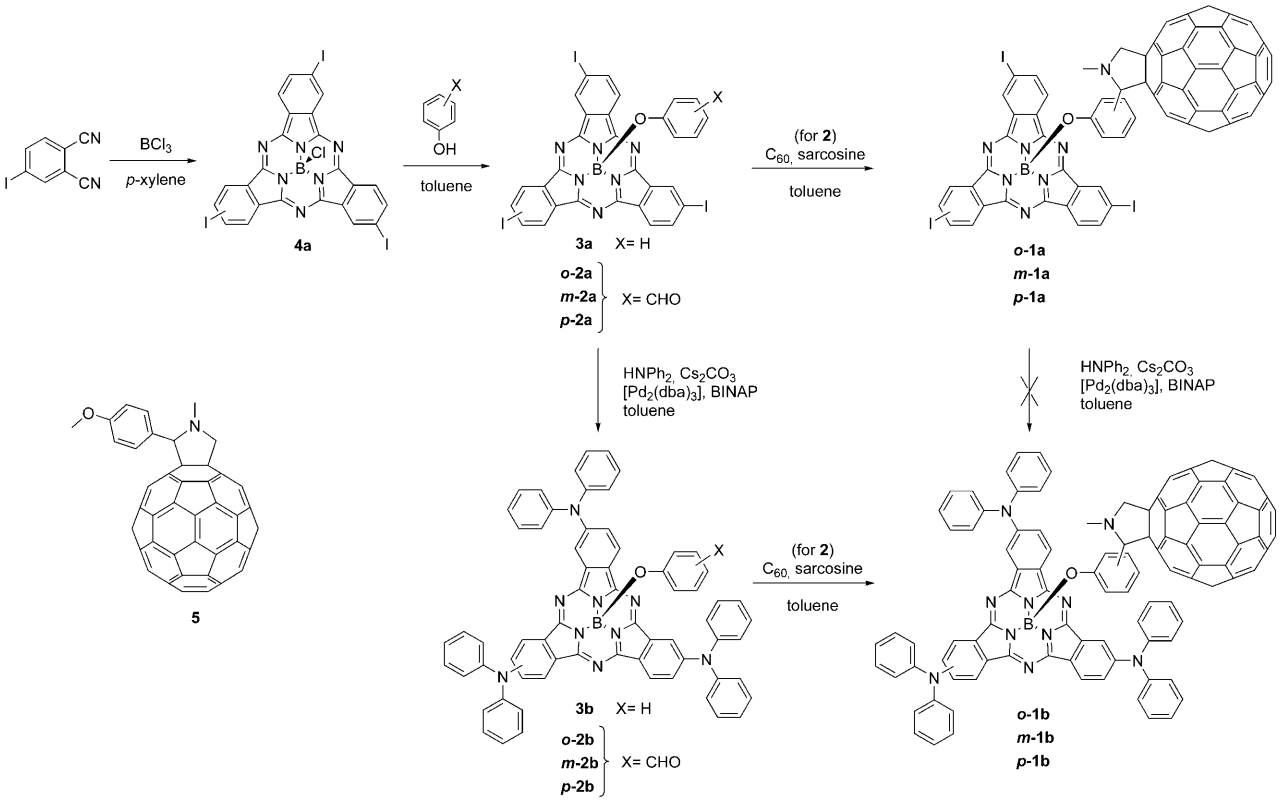

Scheme 1. Synthesis of the two sets of isomeric SubPc-C_{60} (**1a** and **1b**).

 © 2008 Wiley-VCH Verlag GmbH & Co. KGaA, Weinheim

leading to ***o*-2a**, ***m*-2a**, and ***p*-2a**, or by phenol, yielding the reference SubPc **3a**. This set of triiodoSubPc compounds was then subjected to a palladium-catalyzed amination reaction[18] with diphenylamine that afforded ***o*-2b**, ***m*-2b**, ***p*-2b**, and **3b** in nice yields (75–87%). As an alternative to this synthetic route we also examined the direct amination reaction with **4a**, but instead of observing the incorporation of the diphenylamino substituents, the starting chloroSubPc decomposed during these conditions. It seems that an axial phenoxy group imparts chemical stability to the SubPc macrocycle.[19] Finally, ***o*-1a**, ***m*-1a**, ***p*-1a**, ***o*-1b**, ***m*-1b**, and ***p*-1b**, were prepared by 1,3-dipolar cycloaddition reactions[20] between the corresponding SubPc **2a** and **2b** compounds and C_{60}.[21]

Purification was performed by silica gel column chromatography with toluene or toluene/hexane mixtures as eluents. Unreacted fullerene eluted first, followed by the monoaddition compound and a small amount of bisadducts. The corresponding C_3 and C_1 regioisomers of the monoadducts **1a** and **1b** could be separated by column chromatography and were individually characterized.[22] Moreover, in these intrinsically chiral macrocycles, the presence of an additional stereogenic center at the pyrrolidine ring gives rise to a 1:1 mixture of two diastereoisomers for each C_1/C_3 isomer. Only the diastereoisomers of *ortho*-isomeric systems were found to separate in some cases by column chromatography with the conditions employed. Most probably, the restricted rotation—the two subunits being held close by the spacer—is responsible for a greater differentiation between the diastereoisomers.

Evaluation of the relative distance between the SubPc and the C_{60} units: The nature of the phenoxy spacers, which have two torsion angles around σ-bonds that lead to multiple conformations, impart some degree of flexibility to the molecules. This, in turn, means that the C_{60} and SubPc units are not restrained to any fixed relative position, but their distance can shift within a small range. Structural modeling of these systems, using molecular mechanics and semiempirical methods,[23] allowed us to evaluate the maximum and minimum distances between the two moieties in each isomer. These values, defined as the distance between the boron atom and the center of the carbon sphere, together with a model of minimized conformation for each isomer, are illustrated in Figure 1.

The calculated average distances agree quite well with the upfield shifts observed for the signals of the pyrrolidine protons, especially when considering the signal of the proton on the tertiary carbon atom (proton a, Figure 1). In fulleropyrrolidine **5** this proton signal appears as a singlet at $\delta =$ 4.88 ppm. In ***o*-1b**, ***m*-1b**, and ***p*-1b**, on the other hand, the same signal is shifted upfield to $\delta = 3.81$, 4.39, and 4.44 ppm, respectively. A distance-dependent interaction with the SubPc ring-current is responsible for this trend. Similar effects were observed for the corresponding protons in ***o*-1a**, ***m*-1a**, and ***p*-1a** at $\delta = 3.90$, 4.52, and 4.60 ppm, respectively. Furthermore, a significant broadening of the proton signals

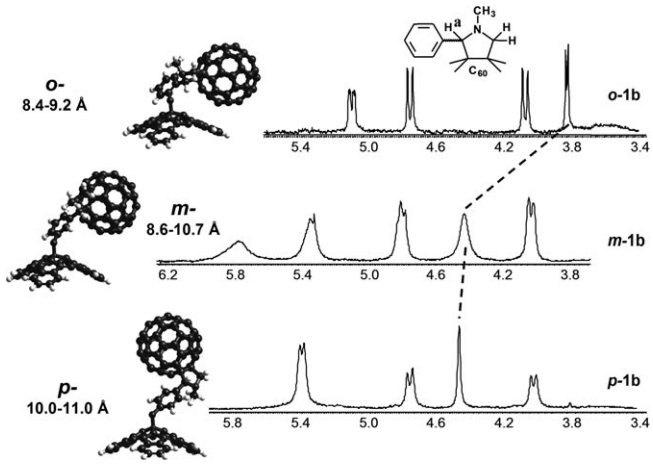

Figure 1. Models and estimated range of interchromophoric distances for *o*-, *m*-, and *p*- isomeric SubPc-C_{60}. Portion of the ^{1}H NMR spectra ($CDCl_3$, 300 MHz) of ***o*-1b**, ***m*-1b**, and ***p*-1b**, showing the magnitude of the upfield shift experienced by some of the pyrrolidine protons as a function of their distance to the SubPc macrocycle.

in the spacer of the *meta* isomers seems to reflect an interconversion between different conformations in a time scale comparable to that of the ^{1}H NMR measurements. This must be due to the higher flexibility of the *meta* spacer, which provides a wider distribution of interchromophoric distances than the other two.

Ground state—electronic absorption spectra: The absorption spectra of all systems disclose features of both constituents (Figure S1a in the Supporting Information). For instance, the presence of C_{60} is clearly seen through absorptions in the 250–350 nm range, followed by a weak band around 430 nm. The SubPc unit, on the other hand, dominates the red part of the spectrum, in which the typical Q-bands appear at around 570 or 615 nm for the **a** or **b** series, respectively. This band is responsible for the marked changes in color that ranges from the typical intense magenta to green. In the **b** series, an additional broad band evolves around 450 nm, which is attributed to n–π* transitions of the amine group.

In the dyads, the SubPc Q-band shows a small red shift when compared to the corresponding reference compounds (i.e., **3a** and **3b**). This bathochromic shift (as illustrated in Figure S1b in the Supporting Information for ***o*-1b**, ***m*-1b**, and ***p*-1b**) slightly weakens as the distance between the two constituents increases. This trend was qualitatively reproduced in several solvents, that is, toluene, $CHCl_3$, THF, or even benzonitrile, and seems to indicate a distance-dependent perturbation of the π–π* SubPc transition by the fullerene unit. Moreover, in the diphenylamine-substituted series the magnitude of the red shift shows a solvent dependence, and an increase in solvent polarity evokes an additional red shift of the SubPc Q-bands (Figure S1c in the Supporting Information).

 © 2008 Wiley-VCH Verlag GmbH & Co. KGaA, Weinheim

Ground state—electrochemistry: Cyclic voltammetry experiments have been carried out with ***o*-1a**, ***m*-1a**, ***p*-1a**, ***o*-1b**, ***m*-1b**, and ***p*-1b**, and compared to the references **3a**, **3b** and **5**. In Table 1 the redox potentials (as measured with this technique) are summarized, while Figure 2 displays the cyclic voltammograms in THF.

Table 1. Potential data (mV vs. ferrocene) for SubPc-C_{60} dyads **1** and reference compounds **3** and **5** in THF.

	E^3_{ox} [a]	E^2_{ox} [a]	E^1_{ox} [a]	$E^1_{1/2,red}$	$E^2_{1/2,red}$	$E^3_{1/2,red}$	HOMO–LUMO[b]
3a			+821	−1323	−1900[a] (=3e)		
***o*-1a**			+822	−1016	−1393	−1560	1.84
***m*-1a**		+998	+779	−1004	−1347	−1511	1.78
***p*-1a**		+1038	+854	−1037	−1380	−1567	1.89
3b	+824	+616	+374	−1579	−2079	−2750[a] (=3e)	
***o*-1b**	+846	+606	+436	−1025	−1567 (2e)	−2153	1.46
***m*-1b**	+840	+586	+372	−1017	−1532 (2e)	−2162	1.39
***p*-1b**	+846	+623	+378	−1028	−1543 (2e)	−2180	1.41
5				−910	−1435	−2019	

[a] Electrochemically irreversible wave. Only peak potentials are given. [b] Estimated HOMO–LUMO energy gap (in eV) as the difference between the first oxidative and reductive potentials of the dyads.

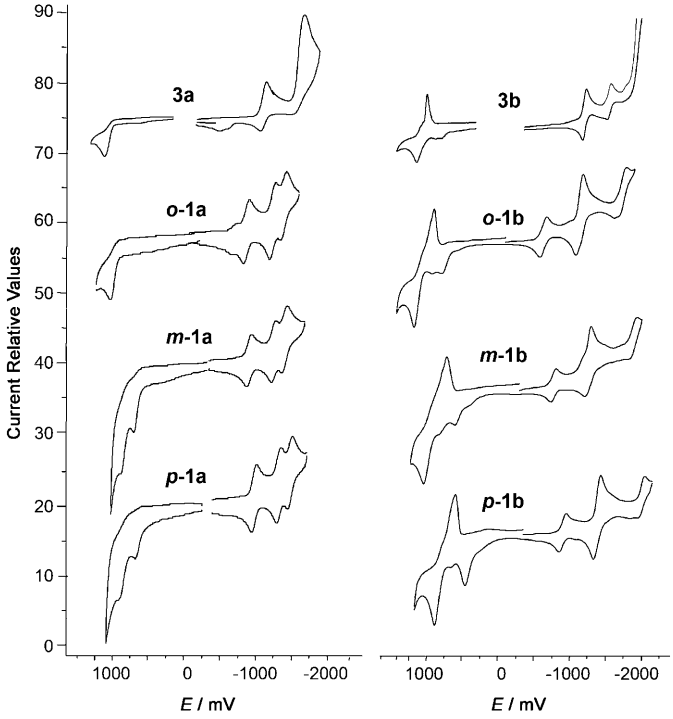

Figure 2. Cyclic voltammograms (mV vs. ferrocene) of references **3a** and **3b** and ***o*-1a**, ***m*-1a**, ***p*-1a**, ***o*-1b**, ***m*-1b**, and ***p*-1b** in THF and 0.1 M $TBAPF_6$ as supporting electrolyte.

For the *o*-, *m*-, and *p*-dyads (**1a**), the cathodic waves at ≈ -1 V ($E^1_{1/2,red}$) and ≈ -1.5 V ($E^3_{1/2,red}$)—one electron each—are assigned to C_{60}, while those seen at $\approx +0.8$ V ($E^1_{p,ox}$) and ≈ -1.4 V ($E^2_{1/2,red}$)—one electron each—are centered on the SubPc. All three reduction processes were found to be fully reversible. On the other hand, the first and the second anodic oxidation processes of ***m*-1a** and ***p*-1a** are irreversible. The second oxidation wave at around +1 V seems to correspond to the oxidation of the nitrogen atom in the pyrrolidine ring attached to the C_{60} group. In the remaining compounds, this oxidation is placed close to the solvent threshold and, in turn, barely observed. The cyclic voltammograms of **3a** also display an irreversible many electron wave reduction ($\approx$3e) at around −1900 mV ($E^2_{p,red}$). A similar wave is observed for **1a** (not shown).

In the case of the diphenylamino series, the first macrocycle-based oxidation was detected at +0.37 V. It displays the usual electrochemical irreversibility seen during the oxidations of SubPc. When scanning to more positive potentials, the **b** series exhibits a second irreversible event around +0.6 V. A three-electron quasi-reversible wave suggests here an oxidation of the diphenylamino groups. After a full oxidation scan strong adsorption at the working electrode evolves, which leads to a green–blue film on the surface. This hampered any further reductive electrochemistry from being detected. The oxidative deposition, which very closely resembles surface-confined behavior, is depicted in Figure S2 (Supporting Information). This behavior was also observed in **1b** and is an interesting property that could be explored in the preparation of thin films.

As far as the cathodic part of **1b** is concerned, the wave at ≈ -1 V ($E^1_{1/2,red}$), corresponding to one electron, was assigned to C_{60}. The wave at ≈ -1.5 V ($E^2_{1/2,red}$), a two-electron process, seems to involve the first reduction of SubPc and the second reduction of C_{60}. The third reduction wave at approximately −2.1 V (one electron) could not definitely be assigned to one or the other of the electroactive species. Following this third reduction process, the observation of the multielectronic (=3e) irreversible reduction of the SubPc at −2.7 V precluded further assignments from the cyclic voltammograms. However, Osteryoung square-wave voltammetry (OSWV; see Figure S3) reveals the close spatial proximity between forming the tetra- and penta-anionic species in these molecules. Adding a third electron to C_{60} and a second electron to SubPc ring appears to happen nearly simultaneously. The order that these events follow is not clearly established nor is the reversibility of the processes, due to the imminent presence of the irreversible multielectronic reduction of the SubPc fragment at around −2.7 V.

Comparing the redox potentials of the *ortho*-, *meta*-, and *para*- isomeric **1a** and **1b** revealed that, in both series, a *meta*-configured spacer induces easier reduction and oxidation of the two electroactive subunits. This is also reflected in the corresponding HOMO/LUMO energy gaps. As shown in Table 1, the lowest values in both series were seen for the *meta*-substituted ***m*-1a** and ***m*-1b**, indicating the weakest interactions between the donor and acceptor groups in each series. Therefore, the electronic effects that influence these ground-state redox processes seem to take place by means of through-bond rather than through-space

 © 2008 Wiley-VCH Verlag GmbH & Co. KGaA, Weinheim

interactions, since they follow the expected (and similar) behavior for the *ortho* and *para*, and the weakest electronic coupling for the *meta* isomer.

Excited states—steady-state and time-resolved fluorescence spectroscopy: First insight into excited-state interactions between the photo- and redox-active constituents came from steady-state and time-resolved fluorescence experiments, in which SubPc was excited either at 570 (i.e., **1a**) or 615 nm (i.e., **1b**). A strong decrease in the SubPc fluorescence intensity is noted when contrasting the results for the dyads (i.e., **1a** and **1b**, quantum yields on the order of 10^{-3}) with those of the references (i.e., **3a** and **3b**, quantum yields on the order of 10^{-1}). Both the fluorescence quantum yields and the fluorescence lifetimes were typically two orders of magnitude lower in the dyads (see Table 2).[24]

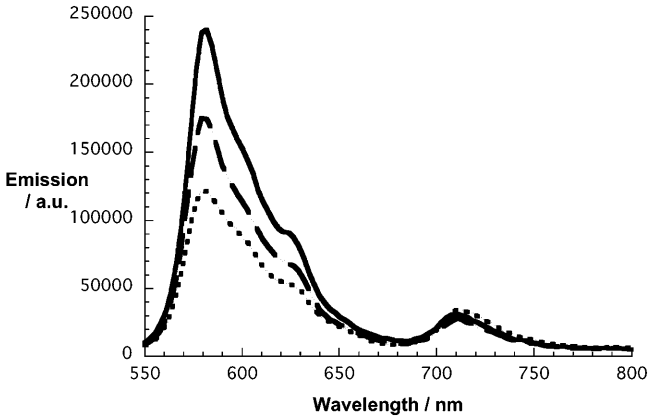

Figure 3. Steady-state fluorescence spectra of ***o*-1a** (dotted spectrum), ***m*-1a** (dashed spectrum), and ***p*-1a** (solid spectrum) in toluene exhibiting the same absorption of 0.15 at the 530 nm excitation wavelength.

Table 2. Selected photophysical parameters of SubPc-C_{60} dyads **1a** and **1b** as a function of solvent and isomeric connection between the two chromophores.

Feature	Solvent	*o*-1a	*m*-1a	*p*-1a	*o*-1b	*m*-1b	*p*-1b
fluorescence maximum [nm]	toluene	596	592	591	654	655	658
fluorescence quantum yield (SubPc)	toluene	7.3×10^{-4}	7.7×10^{-4}	1.0×10^{-3}	3.7×10^{-2}	2.1×10^{-2}	5.1×10^{-3}
	THF	1.1×10^{-3}	1.2×10^{-3}	1.3×10^{-3}	[a]	[a]	[a]
fluorescence quantum yield (C_{60})	toluene	6.6×10^{-4}	4.7×10^{-4}	6.0×10^{-4}	$\ll10^{-4}$	$\ll10^{-4}$	$\ll10^{-4}$
	THF	6×10^{-4}	3.610^{-4}	5.4×10^{-4}	$\ll10^{-4}$	$\ll10^{-4}$	$\ll10^{-4}$
singlet lifetime (C_{60}) [ns]	toluene	1.2	1.0	1.1	[a]	[a]	[a]
	THF	1.0	0.9	1.0	[a]	[a]	[a]
singlet lifetime (SubPc) [ps]	toluene	4.2	10.9	13.9	15.1	9.8	11.7
	THF	4.4	[a]	[a]	1.0	1.7	2.9
energy transfer quantum yield	toluene	1.0	0.8	0.85	[c]	[c]	[c]
radical ion pair lifetime [ps]	toluene	[b]	[b]	[b]	4055	4350	>5000
	THF	[b]	[b]	[b]	133	192	319
	bzcn	[b]	[b]	[b]	73	111	235

[a] Not measured. [b] No charge separation was found. [c] No energy transfer was found.

We have previously demonstrated that the SubPc singlet excited states in ***m*-1a** and ***m*-1b** give rise to different reactivity patters in their excited states, namely, energy- versus charge-transfer deactivation.[17b] The most notable results came from solvent dependence. Solvents of different polarity led in ***m*-1a** to marginal changes in the quantum yields. This suggests a nearly activationless fluorescence deactivation. For ***m*-1b**, on the other hand, using a more polar environment amplified the nonradiative deactivation pathway.

The aforementioned trends are reestablished in the two remaining isomers. Noticeable is the impact that the change in distance and electronic coupling exerts on the deactivation rates: *ortho*-substitution in ***o*-1a**, which imposes unequivocally the shortest distance between SubPc and C_{60}, leads to the strongest quenching within the **1a** series, whereas the weakest SubPc fluorescence quenching was seen in the *para*-isomer ***p*-1a** (Figure 3). Such a trend parallels the red-shifts registered in the ground state absorption (see Figure S1 in the Supporting Information).

Mechanistically, upon SubPc excitation in toluene a fluorescence pattern evolves that bears close resemblance with that known for C_{60} (i.e., **5**), that is, a maximum at 720 nm. Furthermore, the excitation spectra of the C_{60} fluorescence discloses features that match the ground state absorption of SubPc and C_{60}. This provides unambiguous evidence for the origin of the C_{60} fluorescence. Tests in solvents, which are more polar than toluene, for example, THF, *o*-dichlorobenzene or benzonitrile, led to the same intensity of the C_{60} fluorescence in the **1a** series. The only differences that were derived correspond to the quantum yields of energy transfer: when employing **5** as a standard with matching absorption at the excitation wavelength the following trend emerges: ***o*-1a** > ***m*-1a** > ***p*-1a** (see Table 2). Implicit is a distance-dependent singlet–singlet energy transfer from the SubPc singlet excited state in **1a** (i.e., 2.1 eV) to C_{60} (i.e., 1.76 eV) that thermodynamically outperforms any charge transfer (i.e., ca. 1.85 eV).

Quite different is the outcome of the fluorescence experiments with ***o*-1b**, ***m*-1b** and ***p*-1b**. Although the strongest quenching is still seen in ***o*-1b** (Figure 4), a considerable decrease of the fluorescence in the more polar media attests to a different mechanism. In **1b** the charge-transfer products are energetically situated around 1.4 eV, which, in turn, would favor the charge-transfer pathway evolving from the SubPc singlet excited state (i.e., 1.9 eV) rather than the energy-transfer scenario.[25]

Excited states—transient absorption spectroscopy: Time-resolved transient absorption measurements provided further details about the deactivation mechanism. Upon 500 nm excitation of **3a**/**1a** and **3b**/**1b**, we observe the singlet excited-state characteristics of the SubPc constituents. In all cases a bleach of the ground state is accompanied by a new transition that develops in the red. For the **3a**/**1a** series maxima and minima evolve around 640 and 574 nm, respectively,

 © 2008 Wiley-VCH Verlag GmbH & Co. KGaA, Weinheim

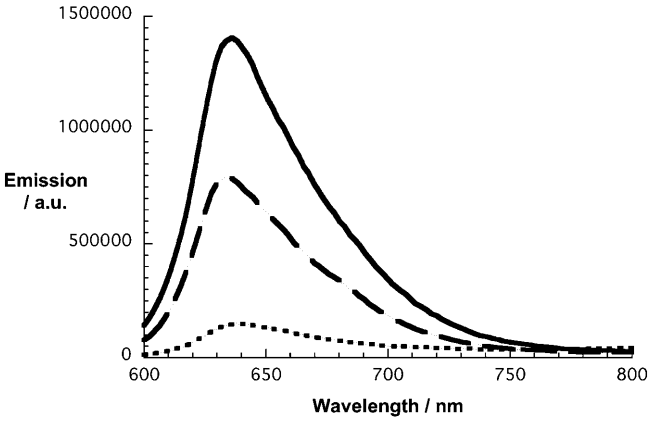

Figure 4. Steady-state fluorescence spectra of ***o*-1b** (dotted spectrum), ***m*-1b** (dashed spectrum), and ***p*-1b** (solid spectrum) in toluene exhibiting the same absorption of 0.24 at the 582 nm excitation wavelength.

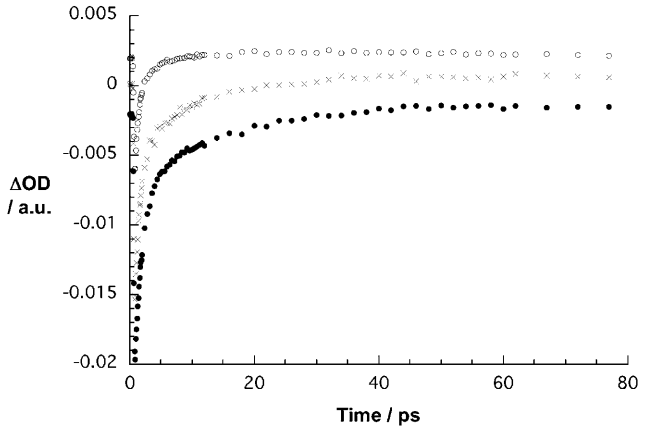

Figure 6. Time-absorption profiles at 560 nm of the differential absorption measurements with ***o*-1a** (open circles), ***m*-1a** (crosses; see also Figure 5), and ***p*-1a** (full circles) in toluene, monitoring the energy-transfer processes.

while the corresponding features for the **3b**/**1b** series are seen at 756 and 615 nm. The intersystem-crossing dynamics are rather slow ($\approx 10^8\ s^{-1}$) in the two references (i.e., **3a** and **3b**). This is in sharp contrast to the ultrafast decays of the SubPc singlet–singlet absorption in **1a** and **1b** with rates $\approx 10^{10}\ s^{-1}$.

In the **1a** series, instead of detecting the transient changes that are associated with the SubPc triplet excited state, we note spectral characteristics that match those seen for **5**, namely, the C_{60} singlet excited state (Figure 5). The most prominent feature is a maximum at 880 nm. Since these C_{60} singlet features develop concomitantly with the decay of the SubPc singlet excited state, we conclude a transduction of singlet-excited-state energy. Appreciable kinetic differences emerge for the different isomers in toluene and THF with energy-transfer rate constants that are larger in ***o*-1a** than in ***m*-1a** and ***p*-1a** (Figure 6). In other words, the underlying distance-dependence resembles that seen in the fluorescence experiments.

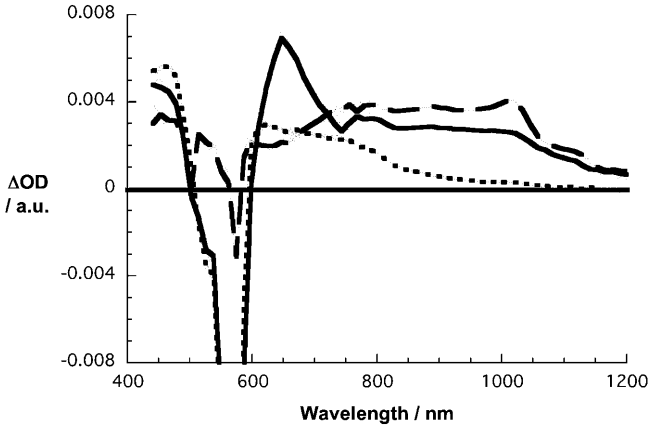

Figure 5. Differential absorption spectra (visible and near-infrared) obtained upon femtosecond flash photolysis (500 nm, 200 nJ) of ***m*-1a** in argon-saturated toluene with time delays of 1.1 ps (solid spectrum), 44 ps (dashed spectrum) and 2472 ps (dotted spectrum) at room temperature, illustrating the sequence of singlet–singlet energy transfer, intersystem crossing, and triplet–triplet energy transfer.

The C_{60} singlet excited state intersystem crosses to the corresponding triplet manifold with dynamics that are virtually identical to that in **5**. Despite this close kinetic agreement, spectroscopically the differential absorption changes are no match to that of the C_{60} triplet excited state (i.e., maxima at 360 and 700 nm). Maxima at 460 and 620 nm and a minimum at 570 nm suggest that the C_{60} singlet decay affords the SubPc triplet excited state. Likewise, the only component detected in the nanosecond experiments was that of the SubPc triplet excited state. Implicit is that the fullerene triplet (1.5 eV), once formed by intersystem crossing, undergoes a thermodynamically allowed, but kinetically not resolvable, transfer of triplet energy to generate the SubPc triplet excited state ($\approx$1.45 eV). The underlying kinetics are affected by the isomeric form and tend to be faster for ***m*-1a** than for ***p*-1a** and ***o*-1a**. Such a trend contrasts the reactivity of singlet–singlet energy transfer.

Different are the results with ***o*-1b**, ***m*-1b**, and ***p*-1b** (see Figure 7 and 8). The SubPc singlet-excited-state features change rapidly into a broadly absorbing species. In the visible region the one-electron-oxidized radical cation of the SubPc donor evolves with maxima at 750 nm, while in the near-infrared region the signature (1000 nm) of the one-electron-reduced radical anion of the C_{60} acceptor. Taken these attributes into concert, there is no doubt about the successful formation of $SubPc^{\bullet+}$–$C_{60}^{\bullet-}$. As already mentioned, better donating abilities in the **1b** series enables the highly efficient (>90%) separation of charges, which is thermodynamically prohibited in the **1a** series. Figure 8 corroborates that in toluene the ***o*-1b**, ***m*-1b**, and ***p*-1b** isomers give rise to appreciable differences in charge-transfer kinetics: ***m*-1b** > ***p*-1b** > ***o*-1b**. Inductive effects are responsible for the diverse rate constants. In fact, these values agree well with the thermodynamic driving force (i.e., HOMO–LUMO gaps), which were derived from the electrochemical experiments. In THF, in which the thermodynamic driving forces for the charge-transfer kinetics (i.e., around 0.5 eV) are brought closer to the top of the Marcus parabola (i.e., on

 © 2008 Wiley-VCH Verlag GmbH & Co. KGaA, Weinheim

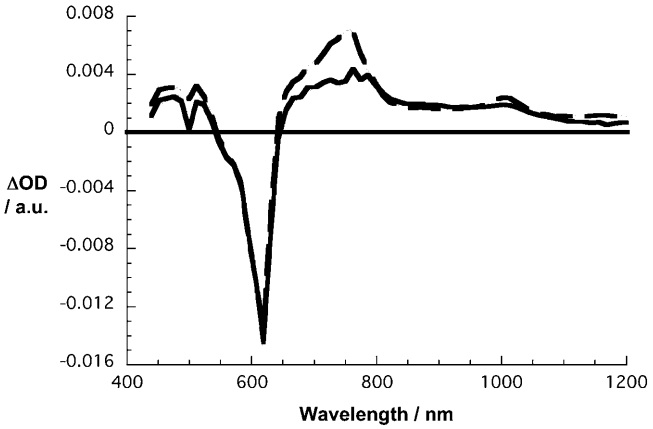

Figure 7. Differential absorption spectra (visible and near-infrared) obtained upon femtosecond flash photolysis (500 nm, 200 nJ) of ***m*-1b** in argon-saturated toluene with time delays of 1.1 ps (solid spectrum) and 24 ps (dashed spectrum) at room temperature, illustrating the charge transfer.

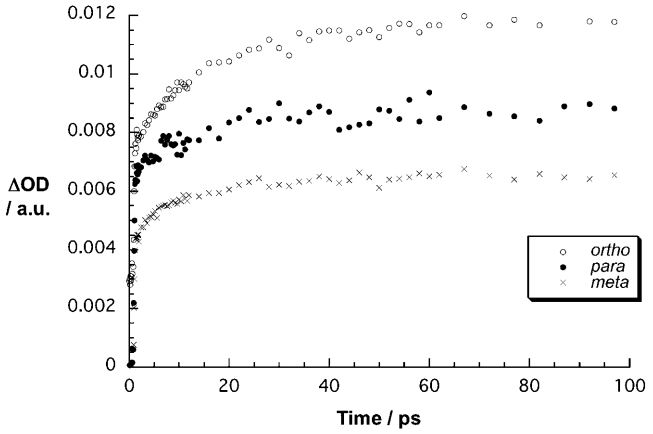

Figure 8. Time-absorption profiles at 750 nm of the differential absorption measurements with ***o*-1b** (open circles), ***m*-1b** (crosses; see also Figure 7), and ***p*-1b** (full circles) in toluene, monitoring the charge-transfer processes.

the order of 0.6 eV as in phthalocyanine–C_{60} and porphryin–C_{60}),[4,26] the rate constants increase relative to those measured in toluene.

Charge recombination leads to the recovery of the ground state for ***o*-1b**, ***m*-1b**, and ***p*-1b**, since the $SubPc^{\bullet+}$–$C_{60}^{\bullet-}$ energy levels (i.e., 1.4–1.2 eV) are presumably situated below those of both triplets (i.e., SubPc and C_{60}). The kinetics of charge recombination are strongly dependent on the solvent polarity and on the isomeric form. Determining the $SubPc^{\bullet+}$-$C_{60}^{\bullet-}$ lifetimes in the different solvents for ***o*-1b**, ***m*-1b**, and ***p*-1b** (Table 2) brought the following trends to light: Firstly, increasing the solvent polarity decreases the $SubPc^{\bullet+}$–$C_{60}^{\bullet-}$ lifetime despite a better solvation of the radical ions: several thousands of picoseconds in toluene and several hundreds of picoseconds in THF, and about hundred picoseconds in benzonitrile. This is a clear attribute of the inverted region of the Marcus parabola, the thermodynamic maximum of which is located between 0.5 and 0.6 eV.[4,27] Please note the rather large driving force for the charge recombination, which is on the order of 1.4 eV. Secondly, decreasing the distance between donor and acceptor decreases the $SubPc^{\bullet+}$–$C_{60}^{\bullet-}$ lifetime despite the opposite effects in the charge separation—exceeding a factor of two when contrasting ***o*-1b** and ***p*-1b**.

Conclusion

The current work demonstrates the impact that a partially conjugated spacer exerts on the ground- and excited-state communication between electron/energy donor and acceptor units in two complementary sets of SubPc–C_{60} systems.

Perturbations of the electronic transitions, caused by the proximity of the two π-conjugated units, dominate the ground state. Additional electrochemical experiments reveal that the HOMO–LUMO gaps tend to be smaller in the *meta*-isomers when compared to those in the corresponding *ortho*- and *para*-isomers. In summary, through-bond interactions play an important role in the electronic communication between the donor and the acceptor in the ground state.

In the excited state, the underlying mechanism, energy (i.e., iodine substituents: **1a**) versus electron transfer (i.e., diphenylamino substituents: **1b**), determines the interactions. Distance matters when dipole–dipole interactions are operative. These govern the transduction of singlet-excited-state energy in **1a**. As a consequence, ***o*-1a** reacts much faster than any of the remaining isomers (i.e., ***p*-1a** and ***m*-1a**). Triplet–triplet energy-transfer reactions, on the other hand, follow a double electron-transfer mechanism, in which inductive effects exert a stronger impact: ***m*-1a** reacts seemingly faster than ***o*-1a** or ***p*-1a**. This conclusion finds independent support in the electrochemical experiments, in which the SubPc oxidation potentials reveal isomer-dependent shifts that suggest through-bond electronic effects.

In the **1b** series, for the initial charge separation a resembling trends evolves, namely, ***m*-1b** undergoes faster charge transfer than ***o*-1b** or ***p*-1b**. It is only for the strongly exothermic charge recombination, again for which distance effects seem to dominate, and the rate constants exhibit the following order: *ortho* > *meta* > *para*.[28]

The reason why this trend differs from previous studies,[11e] in which *meta* isomers showed the slowest charge recombination rates, probably resides in the nature of the phenoxy spacer. This spacer offers more flexibility and poorer electronic coupling than fully π-conjugated spacers.

Experimental Section

General methods: Melting points (m.p.) were determined in a Büchi 504392-S equipment and are uncorrected. UV/Vis spectra were recorded with a Hewlett–Packard 8453 instrument. IR spectra were recorded on a Bruker Vector 22 spectrophotometer. LSI-MS and HRMS spectra were determined on a VG AutoSpec apparatus and MALDI-TOF-MS spectra were obtained from a Bruker Reflex III instrument equipped with a ni-

 © 2008 Wiley-VCH Verlag GmbH & Co. KGaA, Weinheim

trogen laser operating at 337 nm. NMR spectra were recorded with a Bruker AC-300 instrument. Elemental analyses were performed with a Perkin–Elmer 2400 CHN equipment. Column chromatography was carried out on silica gel Merck-60 (230–400 mesh, 60 Å), and TLC on aluminum sheets precoated with silica gel 60 F_{254} (E. Merck). Chemicals were purchased from commercial suppliers and used without further purification.

Electrochemistry: Electrochemical measurements were performed at room temperature in a home-built one-compartment cell with a three-electrode configuration, containing 0.1 M tetrabutylammonium hexafluorophosphate ($TBAPF_6$) as the supporting electrolyte, which was recrystallized twice from ethanol and dried under vacuum. A glassy carbon or gold electrode (3 or 1.5 mm ∅, respectively) was used as the working electrode, and a platinum mesh and a silver wire, separated from the solution by a vycor tip, were employed as the counter and the reference electrodes, respectively. Prior to each voltammetric measurement the cell was degassed and pumped to 10^{-6} mmHg. The solvent, THF (5 mL), which had also been degassed and pumped to the same pressure, was then vapor-transferred into the cell, directly from Na/K. The electrochemical measurements were performed using a concentration of approximately 0.5 mM of the corresponding compound, and ferrocene was added as an internal reference.

Photophysics: Steady-state emission spectra were recorded on a FluoroMax® 3 Fluorometer (HORIBA). The measurements were carried out at room temperature. Fluorescence lifetimes were measured with a Fluorolog® TCSPC system (HORIBA). The samples were excited by a NanoLED-405 LH (peak wavelength 403 nm) and the signal was detected by a Hamamatsu MCP photomultiplier (type R3809U-50). Femtosecond transient absorption studies were performed with 500 nm laser pulses (1 kHz, 150 fs pulse width, 200 nJ) from amplified Ti:Sapphire laser system (Clark-MXR, Inc.).

Standard procedure for the synthesis of SubPcs 2a and 3a: In a 25 mL round-bottomed flask, equipped with a condenser and a magnetic stirrer, the corresponding phenol (2.5 mmol) and SubPc **4a** (0.5 mmol; 404 mg) were heated under reflux in toluene (2 mL) for 40 h (***m*-2a** and ***p*-2a**) or 16 h (**3a**), depending on the reactivity of the starting SubPc and phenol. In the case of ***o*-2a** the reaction was performed in a 10 mL round-bottomed flask, equipped with a magnetic stirrer and rubber seal, in which *o*-hydroxybenzaldehide (1 mmol) and SubPc **4a** were placed. The mixture was heated to the melting point of the phenol and stirred at that temperature for 3 h. Then, in all cases, the reaction mixture was cooled down to room temperature, the solvent was evaporated, and the resulting residue was washed with a 4:1 mixture of methanol/water. The dark magenta solid was then subjected to column chromatography on silica gel using toluene (**3a**) or mixtures of toluene/THF (50:1 for ***o*-2a** or 30:1 for ***m*-2a** and ***p*-2a**). The C_3 and C_1 regioisomers of **2a** were not separated and are characterized below as 3:1 mixtures. All the compounds were further purified by recrystallization from CH_2Cl_2/hexane mixtures. The characterization of SubPcs **3a** and ***m*-2a** has been recently reported.[17b]

SubPc *o*-2a (1:3 mixture of C_3 and C_1 isomers): Compound ***o*-2a** was obtained as a pink solid: 246 mg (55%); m.p. >250 °C; ^{1}H NMR (300 MHz, $CDCl_3$): δ = 9.20 (br s, 3H), 8.94 (s, 1H), 8.55 (d, J_o = 8.2 Hz, 3H), 8.22 (d, J_o = 8.2 Hz, 1H), 7.29 (dd, J_o = 8.1 Hz, J_m = 1.8 Hz, 1H), 7.03 (ddd, J_o = 8.1 Hz, $J_{o'}$ = 7.3 Hz, $J_{m'}$ = 1.8 Hz, 1H), 6.74 (dd, $J_{o'}$ = 7.3 Hz, $J_{o''}$ = 7.6 Hz, 1H), 5.13 ppm (dd, $J_{o''}$ = 7.6 Hz, $J_{m'}$ = 1.8 Hz, 1H); ^{13}C NMR (75.5 MHz, $CDCl_3$): δ = 188.9, 155.4, 151.5, 152.4, 151.2, 150.4, 150.2, 150.0, 139.0, 135.2, 132.2, 129.8, 131.6, 127.9, 123.7, 123.6, 122.1, 119.3, 96.6 ppm; MS (FAB, *m*-NBA): *m/z*: 894 $[M]^+$, 773 $[M-$axial group$]^+$; HRMS: *m/z* calcd for $C_{31}H_{14}N_6O_2BI_3$: 893.8405; found: 893.8517; UV/Vis ($CHCl_3$): λ_{max} (log ε) = 572 (4.5), 532 (sh), 325 (3.9), 273 nm (4.2); FT-IR (KBr): $\tilde{\nu}$ = 1684 (C=O), 1593, 1546, 1433, 1383, 1291, 1260, 1229, 1143, 1041 (B–O), 817, 752, 702 cm^{-1}; elemental analysis calcd (%) for $C_{31}H_{14}N_6O_2BI_3$: C 41.65, H 1.58, N 9.40; found: C 41.24, H 1.67, N 9.36.

SubPc *p*-2a (1:3 mixture of C_3 and C_1 isomers): Compound ***p*-2a** was obtained as a pink solid: 299 mg (67%); m.p. >250 °C; ^{1}H NMR (300 MHz, $CDCl_3$): δ = 9.61 (s, 1H), 9.15 (m, 3H), 8.50 (m, 3H), 8.18 (m, 3H), 7.31 (AA′XX′ system, 2H), 5.44 ppm (AA′XX′ system, 2H); ^{13}C NMR (75.5 MHz, $CDCl_3$): δ = 190.6, 158.1, 151.6, 151.4, 151.2, 150.3, 150.1, 139.0, 132.1, 129.7, 131.6, 131.5, 131.4, 130.3, 123.6, 123.5, 118.8, 96.5 ppm; MS (FAB, *m*-NBA): *m/z*: 894 $[M]^+$, 773 $[M-$axial group$]^+$; HRMS: *m/z* calcd for $C_{31}H_{14}N_6O_2BI_3$: 893.8405; found: 893.8438; UV/Vis ($CHCl_3$): λ_{max} (logε) = 572 (4.5), 531 (sh), 326 (3.9), 274 nm (4.2); FT-IR (KBr): $\tilde{\nu}$ = 1687 (C=O), 1597, 1508, 1459, 1429, 1266, 1176, 1039 (B–O), 818, 779, 755, 701 cm^{-1}; elemental analysis calcd (%) for $C_{31}H_{14}N_6O_2BI_3$: C 41.65, H 1.58, N 9.40; found: C 42.07, H 1.50, N 9.40.

Standard procedure for the synthesis of SubPcs 2b and 3b: An oven-dried 25 mL flask was charged with finely ground Cs_2CO_3 (294 mg, 0.9 mmol), $[Pd_2(dba)_3]$ (8 mg, 0.009 mmol), BINAP (5.6 mg, 0.009 mmol), diphenylamine (152 mg, 0.9 mmol) and the corresponding SubPc (**2a** or **3a** (1:3 mixture of C_3/C_1 regioisomers; 0.1 mmol). The flask was then purged with argon and dry toluene (10 mL) was added through a syringe. The mixture was heated to reflux under argon atmosphere with continuous stirring for 8 h in both cases. The solution was cooled to room temperature, diluted with toluene (20 mL), filtered, and concentrated to about 2–3 mL. The crude product was then purified by flash chromatography on silica gel by using a mixture of hexane/THF (4:1 for **3b** and 3:1 for **2b**) as eluent. The C_3 and C_1 regioisomers of **2b** were not separated and are characterized below as 3:1 mixtures. The resulting deep green solids could be further purified by precipitation from cold hexane. The characterization of SubPcs **3b** and ***m*-2b** has been recently reported.[17b]

SubPc *o*-2b (1:3 mixture of C_3 and C_1 isomers): Compound ***o*-2b** was obtained as a green solid: 70 mg (69%); m.p. >250 °C; ^{1}H NMR (300 MHz, $CDCl_3$): δ = 9.07 (s, 1H), 8.55 (m, 3H), 8.35 (m, 3H), 7.53 (m, 3H), 7.4–7.0 (m, 32H), 6.69 (dd, $J_{o'}$ = $J_{o''}$ = 7.6 Hz, 1H), 5.18 ppm (d, $J_{o''}$ = 7.6 Hz, 1H); ^{13}C NMR (75.5 MHz, $CDCl_3$): δ = 189.7, 156.5, 152.3, 151.5, 150.5, 150.32, 150.27, 150.0, 147.3, 147.2, 135.8, 135.2, 129.7, 129.6, 127.3, 125.5, 125.41, 125.36, 125.2, 124.4, 124.3, 124.2, 123.0, 122.9, 122.8, 121.2, 118.9, 114.4, 114.3, 114.2, 114.1 ppm; MS (FAB, *m*-NBA): *m/z*: 1018 $[M+H]^+$; HRMS: *m/z* calcd for $C_{67}H_{44}N_9O_2B$: 1017.3711; found: 1017.3745; UV/Vis ($CHCl_3$): λ_{max} (logε) = 623 (4.5), 577 (sh), 426 (4.2), 303 (4.6), 255 nm (4.5); FT-IR (KBr): $\tilde{\nu}$ = 1670 (C=O), 1609 (C=N), 1487, 1260, 1195, 1154, 1044 (B–O), 750, 697 cm^{-1}; elemental analysis calcd (%) for $C_{67}H_{44}N_9O_2B$: C 79.05, H 4.36, N 12.38; found: C 78.47, H 4.69, N 12.22.

SubPc *p*-2b (1:3 mixture of C_3 and C_1 isomers): Compound ***p*-2b** was obtained as a green solid: 80 mg (79%); m.p. >250 °C; ^{1}H NMR (300 MHz, $CDCl_3$): δ = 9.63 (s, 1H), 8.55 (m, 3H), 8.35 (m, 3H), 7.54 (m, 3H), 7.4–7.0 (m, 32H), 5.48 ppm (AA′XX′ system, 2H); ^{13}C NMR (75.5 MHz, $CDCl_3$): δ = 190.8, 159.1, 152.5, 151.6, 151.0, 150.6, 150.3, 150.1, 150.0, 149.2, 147.3, 147.23, 147.17, 133.2, 133.0, 132.6, 131.4, 129.74, 129.68, 125.5, 125.4, 125.3, 125.2, 124.4, 124.3, 124.2, 123.0, 122.9, 122.8, 118.7, 114.4, 114.3, 114.2, 114.1 ppm; MS (FAB, *m*-NBA): *m/z*: 1017 $[M]^+$; HRMS: *m/z* calcd for $C_{67}H_{44}N_9O_2B$: 1017.3711; found: 1017.3706; UV/Vis ($CHCl_3$): λ_{max} (logε) = 626 (4.4), 484 (3.8), 436 (3.9), 298 nm (4.5); FT-IR (KBr): $\tilde{\nu}$ = 1696 (C=O), 1601 (C=N), 1480, 1264, 1196, 1156, 1034 (B-O), 751, 697 cm^{-1}; elemental analysis calcd (%) for $C_{67}H_{44}N_9O_2B$: C 79.05, H 4.36, N 12.38; found: C 78.66, H 4.52, N 11.97.

Standard procedure for the synthesis of SubPc-C_{60} dyads 1a and 1b: A solution of C_{60} fullerene (70 mg, 0.1 mmol), *N*-methylglycine (25 mg, 0.27 mmol), and the corresponding (formylphenoxy)SubPc **2a** or **2b** (0.09 mmol) in dry toluene (50 mL) was heated to reflux under argon atmosphere for 20 h (for ***m*-2a**, ***p*-2a**, ***m*-2b**, and ***p*-2b**) or 30 h (for ***o*-2a** and ***o*-2b**). The solution was then cooled to room temperature and concentrated under vacuum to about 10 mL. The resulting mixture was poured onto a silica gel column and eluted with toluene/hexane 5:1 (for compound ***o*-1a**) or toluene (for all the rest of products), in order to separate the monoaddition products from the bisadducts and unreacted fullerene. The C_3 and C_1 regioisomers of all the compounds **1a** and **1b** were separated during chromatography and their individual characterization data is listed below following their elution order. Further purification of the monoadducts was achieved by thoroughly washing the solid products with acetone, methanol and hexane. The characterization of SubPc-C_{60} dyads ***m*-1a** and ***m*-1b** has been recently reported.[17b]

SubPc-C_{60} *o*-1a; C_3 isomer (1:1 mixture of diastereoisomers): Compound ***o*-1a** (C_3) was obtained as a dark red solid: 14 mg (9%); m.p. >250 °C; ^{1}H NMR (300 MHz, $CDCl_3$/CS_2 (1:5)): δ = 9.22, 9.18 (2d, J_m = 1.8 Hz, 3H), 8.57, 8.54 (2d, J_o = 8.2 Hz, 3H), 8,21 (m, 3H), 7.40 (m, 1H), 6.72

 © 2008 Wiley-VCH Verlag GmbH & Co. KGaA, Weinheim

(m, 2H), 4.84 (m, 1H), 4.70 (m, 1H), 3.96 (d, ^2J=9.7 Hz, 1H), 3.91, 3.89 (2s, 1H), 2.32 ppm (s, 3H); MS (MALDI-TOF, dithranol): *m/z*: 1642 $[M+H]^+$; UV/Vis ($CHCl_3$): λ_{max} (logε)=575 (4.4), 525 (sh), 430, 320 (4.2), 262 nm (4.6); FT-IR (KBr): $\tilde{\nu}$=2934, 2922, 1626, 1451, 1344, 1276, 1060 cm^{-1} (B–O); elemental analysis calcd (%) for $C_{93}H_{19}N_7OBI_3$: C 68.04, H 1.17, N 5.97; found: C 67.16, H 1.32, N 6.34.

SubPc-C_{60} *o*-1a; C_1 isomer: Compound ***o*-1a** (C_1) was obtained as a dark red solid: 50 mg (34%). The two diastereoisomers of ***o*-1a** (C_1: α and β) could be isolated and characterized independently by ^{1}H NMR and UV/Vis spectroscopy. For the measuring of melting points, ^{13}C NMR and FT-IR spectroscopy, MS, and elemental analysis, the mixture of diastereoisomers was instead employed. m.p. >250°C; ^{1}H NMR (300 MHz, $CDCl_3$/CS_2 (1:5)): diastereoisomer α: δ=9.20 (m, 3H), 8.55 (m, 3H), 8,21 (m, 3H), 7.39 (m, 1H), 6.71 (m, 2H), 4.82 (m, 1H), 4.69 (d, ^2J=9.3 Hz, 1H), 3.96 (d, ^2J=9.3 Hz, 1H), 3.91 (s, 1H), 2.31 ppm (s, 3H); ^{1}H NMR (300 MHz, $CDCl_3$/CS_2 (1:5)): diastereoisomer β: δ=9.18 (m, 3H), 8.54 (m, 3H), 8.20 (m, 3H), 7.39 (dd, J_o=6.9 Hz, J_m=2.4 Hz, 1H), 6.71 (m, 2H), 4.80 (m, 1H), 4.68 (d, ^2J=9.3 Hz, 1H), 3.94 (d, ^2J=9.3 Hz, 1H), 3.90 (s, 1H), 2.30 ppm (s, 3H); ^{13}C NMR (75.5 MHz, $CDCl_3$/CS_2 (1:5)): δ=138.5, 138.4, 131.6, 131.5, 129.2, 128.6, 123.5, 123.4, 121.8, 116.9, 96.9, 96.5, 78.1, 69.8, 39.6 ppm. The low solubility of this dyad prevented the clear detection of most of the quaternary carbon atom signals, even after 36 h. MS (MALDI-TOF, dithranol): *m/z*: 1642 $[M+H]^+$; UV/Vis ($CHCl_3$): λ_{max} (logε)=575 (4.4), 525 (sh), 430, 320 (4.2), 262 nm (4.6); both diastereoisomers α and β presented the same features. FT-IR (KBr): $\tilde{\nu}$=2934, 2920, 1628, 1449, 1345, 1280, 1059 cm^{-1} (B–O); elemental analysis calcd (%) for $C_{93}H_{19}N_7OBI_3$: C 68.04, H 1.17, N 5.97; found: C 67.30, H 1.26, N 5.72.

SubPc-C_{60} *p*-1a; C_3 isomer (1:1 mixture of diastereoisomers): Compound ***p*-1a** (C_3) was obtained as a dark red solid: 20 mg (14%); m.p. >250°C; ^{1}H NMR (300 MHz, $CDCl_3$/CS_2 (1:5)): δ=9.13–9.07 (2m, 3H), 8.48, 8.43 (2d, J_0=8.2 Hz, 3H), 8,15 (m, 3H), 7.18 (m, 2H), 5.37 (m, 2H), 4.83 (d, ^2J=9.7 Hz, 1H), 4.60 (s, 1H), 4.10 (d, ^2J=9.7 Hz, 1H), 2.59 ppm (s, 3H); MS (MALDI-TOF, dithranol): *m/z*: 1642 $[M+H]^+$; UV/Vis ($CHCl_3$): λ_{max} (logε)=572 (4.4), 522 (sh), 432, 320 (4.2), 260 nm (4.6); FT-IR (KBr): $\tilde{\nu}$= 2974, 2919, 1625, 1453, 1345, 1276, 1061 cm^{-1} (B–O); elemental analysis calcd (%) for $C_{93}H_{19}N_7OBI_3$: C 68.04, H 1.17, N 5.97; found: C 67.29, H 1.19, N 5.59.

SubPc-C_{60} *p*-1a; C_1 isomer (1:1 mixture of diastereoisomers): Compound ***p*-1a** (C_1) was obtained as a dark red solid: 61 mg (42%); m.p. >250°C; ^{1}H NMR (300 MHz, $CDCl_3$/CS_2 (1:5)): δ=9.09 (m, 3H), 8.46 (m, 3H), 8,15 (m, 3H), 7.18 (m, 2H), 5.38 (m, 2H), 4.82 (d, ^2J=9.3 Hz, 1H), 4.59 (s, 1H), 4.09 (d, ^2J=9.3 Hz, 1H), 2.59 ppm (s, 3H); ^{13}C NMR (75.5 MHz, $CDCl_3$/CS_2 (1:5)): δ=138.5, 131.6, 131.5, 129.6, 123.3, 119.0, 96.9, 82.4, 81.8, 68.2, 69.5, 39.5 ppm. The low solubility of this dyad prevented the clear detection of most of the quaternary carbon atom signals, even after 36 h. MS (MALDI-TOF, dithranol): *m/z*: 1642 $[M+H]^+$; UV/Vis ($CHCl_3$): λ_{max} (logε)=572 (4.5), 520 (sh), 432, 320 (4.3), 260 nm (4.7); FT-IR (KBr): $\tilde{\nu}$=2934, 2920, 1628, 1449, 1345, 1280, 1059 cm^{-1} (B–O); elemental analysis calcd (%) for $C_{93}H_{19}N_7OBI_3$: C 68.04, H 1.17, N 5.97; found: C 67.11, H 1.29, N 5.77.

SubPc-C_{60} *o*-1b; C_3 isomer (1:1 mixture of diastereoisomers): Compound ***o*-1b** (C_3) was obtained as a dark green solid: 15 mg (9%); m.p. >250°C; ^{1}H NMR (300 MHz, $CDCl_3$): δ=8.52, 8.49 (2d, J_o=8.6 Hz, 3H), 8.39, 8.37 (2d, J_m=1.8 Hz, 3H), 7.50 (dd, J_o=8.6 Hz, J_m=1.8 Hz, 3H), 7.29 (m, 13H), 7.15 (m, 18H), 6.70 (m, 2H), 5.10 (m, 1H), 4.73 (d, ^2J=9.4 Hz, 1H), 4.05 (d, ^2J=9.4 Hz, 1H), 3.83, 3.79 (2s, 1H), 2.40 ppm (s, 3H); MS (MALDI-TOF, dithranol): *m/z*: 1766 $[M+H]^+$; UV/Vis ($CHCl_3$): λ_{max} (logε)=629 (4.5), 452 (4.1), 434 (4.1), 312 nm (4.8); FT-IR (KBr): $\tilde{\nu}$=2932, 1596, 1480, 1453, 1279, 1185, 1050, 751, 697 cm^{-1}; elemental analysis calcd (%) for $C_{129}H_{49}N_{10}OB$: C 87.75, H 2.80, N 7.93; found: C 86.66, H 2.89, N 7.56.

SubPc-C_{60} *o*-1b; C_1 isomer (1:1 mixture of diastereoisomers): Compound ***o*-1b** (C_1) was obtained as a dark green solid: 49 mg (31%); m.p. >250°C; ^{1}H NMR (300 MHz, $CDCl_3$): δ=8.52 (m, 3H), 8.38 (m, 3H), 7.57 (m, 3H), 7.4–7.0 (m, 31H), 6.70 (m, 2H), 5.10 (m, 1H), 4.74 (d, ^2J= 9.4 Hz, 1H), 4.07 (d, ^2J=9.4 Hz, 1H), 3.84, 3.80 (2s, 1H), 2.41 ppm (s, 3H); ^{13}C NMR (75.5 MHz, $CDCl_3$): δ=155.6, 155.4, 155.2, 153.1, 153.0, 151.84, 151.77, 151.2, 151.0, 150.21, 150.16, 149.8, 149.6, 149.4, 149.3, 148.7, 148.66, 148.5, 146.5, 146.3, 146.2, 146.18, 145.8, 145.6, 145.4, 145.0, 149.7, 144.9, 144.8, 144.73, 144.69, 144.4, 144.2, 143.7, 143.6, 143.5, 143.3, 143.0, 142.6, 142.3, 142.0, 141.6, 141.34, 141.26, 141.0, 140.6, 140.5, 140.4, 139.6, 139.3, 139.0, 138.7, 136.11, 136.06, 135.2, 135.1, 147.5, 147.42, 147.37, 137.0, 133.3, 133.2, 129.7, 129.5, 129.0, 128.6, 125.7, 125.5, 125.4, 124.8, 124.7, 124.5, 124.3, 124.2, 124.1, 124.0, 123.1, 123.0, 121.8, 117.2, 114.33, 114.27, 114.2, 77.6, 69.9, 39.7 ppm; MS (MALDI-TOF, dithranol): *m/z*: 1766 $[M+H]^+$; UV/Vis ($CHCl_3$): λ_{max} (logε)=629 (4.5), 581 (sh), 436 (4.1), 401 (3.9), 306 (4.7), 259 nm (4.9); FT-IR (KBr): ν=2957, 1596, 1480, 1453, 1279, 1185, 1050 (B–O), 751, 697 cm^{-1}; elemental analysis calcd (%) for $C_{129}H_{49}N_{10}OB$: C 87.75, H 2.80, N 7.93; found: C 86.92, H 2.91, N 8.21.

SubPc-C_{60} *p*-1b; C_3 isomer (1:1 mixture of diastereoisomers): Compound ***p*-1b** (C_3) was obtained as a dark green solid: 16 mg (11%); m.p. >250°C; ^{1}H NMR (300 MHz, $CDCl_3$): δ=8.44, 8.42 (2d, J_o=8.8 Hz, 3H), 8.37, 8.29 (2d, J_m=1.8 Hz, 3H), 7.43 (m, 3H), 7.35–7.0 (m, 32H), 5.40 (m, 2H), 4.75 (d, ^2J=9.4 Hz, 1H), 4.50, 4.49 (2s, 1H), 4.03 (d, ^2J= 9.4 Hz, 1H), 2.56, 2.55 ppm (2s, 3H); MS (MALDI-TOF, dithranol): *m/z*: 1766 $[M+H]^+$; UV/Vis ($CHCl_3$): λ_{max} (logε)=624 (4.4), 578 (sh), 433 (4.0), 308 (4.7), 260 nm (4.8); FT-IR (KBr): $\tilde{\nu}$=2977, 1597, 1489, 1260, 1179, 1044 (B–O), 818, 751, 697 cm^{-1}; elemental analysis calcd (%) for $C_{129}H_{49}N_{10}OB$: C 87.75, H 2.80, N 7.93; found: C 86.19, H 2.92, N 7.53.

SubPc-C_{60} *p*-1b; C_1 isomer (1:1 mixture of diastereoisomers): Compound ***p*-1b** (C_1) was obtained as a dark green solid: 57 mg (35%); m.p. >250°C; ^{1}H NMR (300 MHz, $CDCl_3$): δ=8.42 (m, 3H), 8.33, 8.26 (2m, 3H), 7.42 (m, 3H), 7.35–7.0 (m, 32H), 5.37 (m, 1H), 4.73 (d, ^2J=9.4 Hz, 1H), 4.49 (brs, 1H), 4.00 (d, ^2J=9.4 Hz, 1H), 2.56, 2.54 ppm (2s, 3H); ^{13}C NMR (75.5 MHz, $CDCl_3$): δ=155.5, 155.2, 153.3, 153.2, 151.8, 151.7, 151.1, 151.0, 150.2, 150.1, 149.9, 149.7, 149.6, 149.4, 149.3, 148.9, 148.7, 148.5, 146.3, 146.14, 146.08, 145.61, 145.56, 145.3, 145.1, 145.0, 144.94, 144.89, 144.7, 144.5, 144.4, 144.1, 143.9, 143.5, 143.0, 142.3, 142.0, 141.6, 141.31, 141.26, 141.1, 140.9, 140.6, 140.4, 139.3, 139.2, 139.1, 138.8, 136.2, 136.0, 135.0, 134.9, 147.1, 147.0, 137.5, 133.5, 133.4, 133.2, 129.8, 125.5, 125.4, 125.2, 124.7, 124.6, 124.4, 124.2, 124.1, 123.2, 123.1, 123.0, 121.9, 114.5, 114.4, 114.2, 82.6, 69.7, 68.2, 39.6 ppm; MS (MALDI-TOF, dithranol): *m/z*: 1766 $[M+H]^+$; UV/Vis ($CHCl_3$): λ_{max} (logε)=624 (4.5), 578 (sh), 433 (4.1), 308 (4.8), 260 nm (4.9); FT-IR (KBr): $\tilde{\nu}$=2975, 2923, 1599, 1489, 1261, 1181, 1045 (B–O), 818, 750, 699 cm^{-1}; elemental analysis calcd (%) for $C_{129}H_{49}N_{10}OB$: C 87.75, H 2.80, N 7.93; found: C 87.09, H 2.83, N 7.69.

Acknowledgements

Financial support from the Ministerio de Ciencia y Tecnología (CTQ2005–08933/BQU, Consolider-Ingenio 2010 CSD2007–00010 Nanociencia Molecular, ESF-MEC MAT2006–28180-E, SOHYDS), and Comunidad de Madrid (MADRISOLAR, S-0505/PPQ/0225) is gratefully acknowledged (T.T.). This work was also partially supported by the U.S. National Science Foundation, grant DMR-0809129 (L.E.), Deutsche Forschungsgemeinschaft (SFB 583), FCI, and the Office of Basic Energy Sciences of the U.S. Department of Energy (D.M.G.).

[1] *Electron Transfer in Chemistry, Vol. I–V*, (Ed.: V. Balzani), Wiley-VCH, Weinheim, **2001**.
[2] *Molecular Mechanisms of Photosynthesis* (Ed.: R. E. Blankenship), Blackwell Science, Oxford, **2002**.
[3] a) C. Winder, N. S. Sariciftci, *J. Mater. Chem.* **2004**, *14*, 1077–1086; b) S. Guenes, H. Neugebauer, N. S. Sariciftci, *Chem. Rev.* **2007**, *107*, 1324–1338.
[4] a) D. M. Guldi, N. Martín, *J. Mater. Chem.* **2002**, *12*, 1978–1992; b) D. M. Guldi, H. Imahori, *J. Porphyrins Phthalocyanines* **2004**, *8*, 976–983; c) D. M. Guldi, F. Zerbetto, V. Georgakilas, M. Prato, *Acc. Chem. Res.* **2005**, *38*, 38–43; d) D. M. Guldi, G. M. A. Rahman, C. Ehli, V. Sgobba, *Chem. Soc. Rev.* **2006**, *35*, 471–487; e) D. M. Guldi, *Phys. Chem. Chem. Phys.* **2007**, *9*, 1400–1420.

 © 2008 Wiley-VCH Verlag GmbH & Co. KGaA, Weinheim

[5] a) J. M. Tour, *Chem. Rev.* **1996**, *96*, 537–554; b) M. A. Reed, C. Zhou, C. J. Muller, T. P. Burgin, J. M. Tour, *Science* **1997**, *278*, 252–254; c) J. Chen, M. A. Reed, A. M. Rawlett, J. M. Tour, *Science* **1999**, *286*, 1550–1552; d) D. K. James, J. M. Tour, *Top. Curr. Chem.* **2005**, *257*, 33–62.

[6] T. Hayes, M. R. Wasielewski, D. Gosztola, *J. Am. Chem. Soc.* **2000**, *122*, 5563–5567.

[7] W. B. Davis, W. A. Svec, M. A. Ratner, M. R. Wasielewski, *Nature* **1998**, *396*, 60–63.

[8] a) M. Sirish, R. Kache, B. G. Maiya, *J. Photochem. Photobiol. A* **1996**, *93*, 129–136; b) N. V. Tkachenko, H. Lemmetyinen, J. Sonoda, K. Ohkubo, T. Sato, H. Imahori, S. Fukuzumi, *J. Phys. Chem. A* **2003**, *107*, 8834–8844; c) H. Nishikawa, S. Kojima, T. Kodama, I. Ikemoto, S. Susuki, K. Kikuchi, M. Fujitsuka, L. Hongxia, Y. Araki, O. Ito, *J. Phys. Chem. A* **2004**, *108*, 1881–1890.

[9] a) H. A. Kramers, *Physica* **1934**, *1*, 182–192; b) M. Bixon, J. Jortner, M. E. Michel-Beyerle, A. Ogrodnik, *Biochim. Biophys. Acta* **1989**, *977*, 273–286.

[10] a) D. Gust, T. A. Moore, A. L. Moore, C. Devadoss, P. A. Liddell, R. Hermant, R. A. Nieman, L. J. Demanche, J. M. DeGraziano, I. Gouni, *J. Am. Chem. Soc.* **1992**, *114*, 3590–3603; b) A. Harriman, F. M. Romero, R. Ziessel, *J. Phys. Chem. A* **1999**, *103*, 5399–5408.

[11] a) H. Imahori, K. Hagiwara, M. Aoki, T. Akiyama, S. Taniguchi, T. Okada, M. Shirakawa, Y. Sakata, *J. Am. Chem. Soc.* **1996**, *118*, 11771–11782; b) S. Shinoda, H. Tsukube, Y. Nishimura, I. Yamazaki, A. Osuka, *Tetrahedron* **1997**, *53*, 13657–13666; c) A. Stockmann, J. Kurzawa, N. Fritz, N. Acar, S. Schneider, J. Daub, R. Engl, T. Clark, *J. Phys. Chem. A* **2002**, *106*, 7958–7970; d) S. Shaakov, T. Galili, E. Stavitski, H. Levanon, A. Lukas, M. R. Wasielewski, *J. Am. Chem. Soc.* **2003**, *125*, 6563–6572; e) A. L. Thompson, T.-S. Ahn, K. R. J. Thomas, S. Thayumanavan, T. J. Martínez, C. J. Bardeen, *J. Am. Chem. Soc.* **2005**, *127*, 16348–16349.

[12] J. J. Sunner, S. E. Creager, *J. Am. Chem. Soc.* **2000**, *122*, 11914–11920.

[13] a) K. M. Gaab, A. L. Thompson, J. Xu, T. J. Martinez, C. J. Bardeen, *J. Am. Chem. Soc.* **2003**, *125*, 9288–9289; b) A. L. Thompson, K. M. Gaab, J. Xu, C. J. Bardeen, T. J. Martinez, *J. Phys. Chem. A* **2004**, *108*, 671–682.

[14] a) D. E. Richardson, H. Taube, *J. Am. Chem. Soc.* **1983**, *105*, 40–51; b) V. Marvaud, J.-P. Launay, C. Joachim, *Chem. Phys.* **1993**, *177*, 23–30; c) B. P. Paulson, L. A. Curtiss, B. Bal, G. L. Closs, J. R. Miller, *J. Am. Chem. Soc.* **1996**, *118*, 378–387; d) C. Patoux, C. Coudret, J.-P. Launay, C. Joachim, A. Gourdon, *Inorg. Chem.* **1997**, *36*, 5037–5049; e) C. Patoux, J.-P. Launay, M. Beley, S. Chodorowsky-Kimmes, J.-P. Collin, S. James, J.-P. Sauvage, *J. Am. Chem. Soc.* **1998**, *120*, 3717–3725; f) C. Rovira, D. Ruíz-Molina, O. Elsner, J. Vidal-Gancedo, J. Bonvoisin, J.-P. Launay, J. Veciana, *Chem. Eur. J.* **2001**, *7*, 240–250; g) V. Lloveras, J. Vidal-Gancedo, D. Ruíz-Molina, T. M. Figueira-Duarte, J.-F. Nierengarten, J. Veciana, C. Rovira, *Faraday Discuss.* **2006**, *131*, 291–305.

[15] a) A. Meller, A. Ossko, *Monatsh. Chem.* **1972**, *103*, 150–155; seminal work in this area was done by N. Kobayashi, see, for example: b) N. Kobayashi, R. Kondo, S. Nakajima, T. Osa, *J. Am. Chem. Soc.* **1990**, *112*, 9640–9641; relevant reviews can be found in: c) M. Geyer, F. Plenzig, J. Rauschnabel, M. Hanack, B. del Rey, A. Sastre, T. Torres, *Synthesis* **1996**, 1139; d) C. G. Claessens, D. González-Rodríguez, T. Torres, *Chem. Rev.* **2002**, *102*, 835–853; e) "Synthesis and Spectroscopic Properties of Phthalocyanine Analogs": N. Kobayashi, in *The Porphyrin Handbook Vol. 15*, (Eds.: K. M. Kadish, K. M. Smith, R. Guilard), Academic Press, San Diego, CA, **2003**, pp. 161–262; f) T. Torres, *Angew. Chem.* **2006**, *118*, 2900–2903; *Angew. Chem. Int. Ed.* **2006**, *45*, 2834–2837; g) G. de la Torre, C. G. Claessens, T. Torres, *Chem. Commun.* **2007**, 2000–2015.

[16] a) N. Kobayashi, T. Ishizaki, K. Ishii, K. Konami, *J. Am. Chem. Soc.* **1999**, *121*, 9096–9110; b) C. G. Claessens, T. Torres, *Tetrahedron Lett.* **2000**, *41*, 6361–6365; c) C. G. Claessens, T. Torres, *Angew. Chem.* **2002**, *114*, 2673–2677; *Angew. Chem. Int. Ed.* **2002**, *41*, 2561–2565; d) T. Fukuda, J. R. Stork, R. J. Potucek, M. M. Olmstead, B. C. Noll, N. Kobayashi, W. S. Durfee, *Angew. Chem.* **2002**, *114*, 2677–2680; *Angew. Chem. Int. Ed.* **2002**, *41*, 2565–2568; for nonlinear optical properties see: e) A. Sastre, T. Torres, M. A. Díaz-García, F. Agulló-López, C. Dhenaut, S. Brasselet, I. Ledoux, J. Zyss, *J. Am. Chem. Soc.*, **1996**, *118*, 2746–2747; f) B. del Rey, U. Keller, T. Torres, G. Rojo, F. Agulló-López, S. Nonell, C. Martí, S. Brasselet, I. Ledoux, J. Zyss, *J. Am. Chem. Soc.* **1998**, *120*, 12808–12817; g) G. de la Torre, P. Vázquez, F. Agulló-López, T. Torres, *J. Mater. Chem.* **1998**, *8*, 1671–1683; h) G. de la Torre, P. Vázquez, F. Agulló-López, T. Torres, *Chem. Rev.* **2004**, *104*, 3723–3750.

[17] SubPcs are the subject of increasing attention as electron and/or energy donors/acceptors in molecular systems. a) D. González-Rodríguez, T. Torres, D. M. Guldi, J. Rivera, L. Echegoyen, *Org. Lett.* **2002**, *4*, 335–338; b) D. González-Rodríguez, T. Torres, M. A. Herranz, J. Rivera, L. Echegoyen, D. M. Guldi, *J. Am. Chem. Soc.* **2004**, *126*, 6301–6313; c) D. González-Rodríguez, C. G. Claessens, T. Torres, S. Liu, L. Echegoyen, N. Vila, S. Nonell, *Chem. Eur. J.* **2005**, *11*, 3881–3893; d) D. González-Rodríguez, T. Torres, M. M. Olmstead, J. Rivera, M. A. Herranz, L. Echegoyen, C. Atienza Castellanos, D. M. Guldi, *J. Am. Chem. Soc.* **2006**, *128*, 10680–10681; e) R. S. Iglesias, C. G. Claessens, G. M. A. Rahman, M. A. Herranz, D. M. Guldi, T. Torres, *Tetrahedron* **2007**, *63*, 12396–12404; f) M. E. El-Khouly, S. H. Shim, Y. Araki, O. Ito, K.-Y. Kay, *J. Phys. Chem. B* **2008**, *112*, 3910–3917; g) A. Medina, C. G. Claessens, G. M. A. Rahman, A. M. Lamsabhi, O. Mo, M. Yañez, D. M. Guldi, T. Torres, *Chem. Commun.* **2008**, 1759–1761.

[18] a) J. F. Hartwig, *Angew. Chem.* **1998**, *110*, 2154–2177; *Angew. Chem. Int. Ed.* **1998**, *37*, 2046–2067; b) B. H. Yang, S. L. Buchwald, *J. Organomet. Chem.* **1999**, *576*, 125–146.

[19] C. G. Claessens, D. González-Rodríguez, B. del Rey, T. Torres, G. Mark, H.-P. Schuchmann, C. von Sonntag, J. G. MacDonald, R. S. Nohr, *Eur. J. Org. Chem.* **2003**, 2547–2551.

[20] a) M. Prato, M. Maggini, *Acc. Chem. Res.* **1998**, *31*, 519–526; b) N. Tagmatarchis, M. Prato, *Synlett* **2003**, *6*, 768–779.

[21] Carrying out the palladium-catalyzed amination reaction on SubPc-C_{60} compounds **1a** did not yield any product, presumably by inactivation of the catalyst due to coordination to the C_{60} unsaturated sphere; see: A. L. Balch, M. M. Olmstead, *Chem. Rev.* **1998**, *98*, 2123–2165.

[22] The electrochemical and photophysical studies were performed on a 1:3 mixture of C_3/C_1 regioisomers, due to their almost identical physical properties.

[23] Structural modeling was performed using the Hyperchem 6.03 package (Hypercube, Inc.) for Windows.

[24] Detection of the subphthalocyanine fluorescence was hampered in some cases (dyads **1a**) by the instrumental time resolution (< 100 ps).

[25] When turning to time-resolved fluorescence measurements the only detectable component was that of C_{60} with lifetimes that in ***o*-1a**, ***m*-1a**, and ***p*-1a** are superimposable to that of **5**; however, no such C_{60} component was seen in ***o*-1b**, ***m*-1b**, and ***p*-1b**.

[26] a) D. M. Guldi, *Pure Appl. Chem.* **2003**, *75*, 1069–1075; b) H. Imahori, *Org. Biomol. Chem.* **2004**, *2*, 1425–1433; c) S. Fukuzumi, *Funct. Org. Mater.* **2007**, 465–510.

[27] a) D. M. Guldi, A. Gouloumis, P. Vázquez, T. Torres, V. Georgakilas, M. Prato, *J. Am. Chem. Soc.*, **2005**, *127*, 5811–5813; b) M. Quintiliani, A. Kahnt, T. Wölfle, W. Hieringer, P. Vázquez, A. Görling, D. M. Guldi, T. Torres, *Chem. Eur. J.* **2008**, *14*, 3765–3775.

[28] Notable is, nevertheless, that the charge recombination is not quantitative. For example, at the end of the femtosecond timescale a residual absorbance persists that lasts well into the nanosecond regime. The overall yield of this long-lived product is about 10%.

Received: May 13, 2008
Published online: July 15, 2008

 © 2008 Wiley-VCH Verlag GmbH & Co. KGaA, Weinheim